Chemical Engineering Journal 162 (2010) 821–828

Contents lists available at ScienceDirect

Chemical Engineering Journal

journal homepage: www.elsevier.com/locate/cej

3D CFD simulation of hydrodynamics of a 150 MW_e circulating fluidized bed boiler

Nan Zhang[a,b], Bona Lu[a,b], Wei Wang[a,*], Jinghai Li[a]

[a] Institute of Process Engineering, Chinese Academy of Sciences, Zhongguancun Beiertiao 1, Haidian District, Beijing 100190, China
[b] Graduate University of the Chinese Academy of Sciences, Beijing 100049, China

ARTICLE INFO

Article history:
Received 5 February 2010
Received in revised form 23 June 2010
Accepted 25 June 2010

Keywords:
CFD
Circulating fluidized bed
Multiphase flow
Simulation
Fluidization
Hydrodynamics

ABSTRACT

An Eulerian granular multiphase model with a drag coefficient based on the energy minimization multi-scale (EMMS) model was used to perform a three-dimensional (3D), full-loop, time-dependent simulation of hydrodynamics of a 150 MW_e circulating fluidized bed (CFB) boiler. Simulation results were presented in terms of the pressure profile around the whole loop of solids circulation, profiles of solids volume fraction and solids vertical velocity, as well as the non-uniform distribution of solid fluxes into two parallel cyclones.

1. Introduction

Owing to the advantages of low emission and fuel flexibility, circulating fluidized bed (CFB) boilers for utility power generation have been increasing in the past decades in both capacity and quantity. Proper design and scale-up of a CFB boiler rely heavily on its hydrodynamic understanding. To this end, experimentation is certainly an approach, while numerical simulation is another, receiving growing interest with the rapid development of computational technologies, especially computational fluid dynamics (CFD).

Reported simulations of CFB boilers in literature are mostly based on empirical models, from which we can see a growing complexity in terms of multiphase flow hydrodynamics. For example, starting with a combination of zero-dimensional solid mass balance model and a one-dimensional (1D) gaseous and solid species model [1], Hyppänen's group have recently turned to three-dimensional (3D) description of gaseous and solid species [2–4] and presented simulations of different boilers ranging from 15 MW_e [2], 235 MW_e [3], up to 460 MW_e utility facilities [4]. Based on empirical flow distribution and combustion behavior in the furnace, Werther's group have developed a comprehensive, 3D boiler model involving primary fragmentation, char population balance, devolatilization and combustion, etc. [5–7], in which the furnace was divided into four zones according to the flow characteristics, each with individual module. This model has been applied to a 12 MW_{th} boiler constructed in Chalmers University of Technology, Sweden. The influence of mixing and geometry on the overall performance was emphasized with validation against measured data. Pallares and Johnsson [8,9] divided CFB boiler into six zones in their reports, reflecting different understanding of the hydrodynamics inside boilers. In practice, how to appropriately describe the hydrodynamics with empirically reduced models remains a challenge, especially for the complex system like a CFB boiler with strong coupling between different zones around its entire loop.

CFD simulation enables more detailed hydrodynamics description and thus receives growing attentions in recent years [10–12]. Flour and Boucker [10] reported simulations of an industrial CFB test-rig by using the code ESTET-ASTRID, in which they proposed a new definition of mean diameter to better close the drag force and introduced a porosity model estimating the pressure drop on the fluidization regime. Xiao [11] presented a CFD simulation of a 135 MW_e CFB boiler with a corrected drag force model, and compared his results with measured data. Hartge et al. [12] presented 3D CFD simulations of a pilot-scale CFB riser with rectangular cross section and found those simulations with a drag coefficient correlation from the energy-minimization multi-scale (EMMS) model predicted the dense bottom zone very well.

Current CFD simulations are usually performed only for the furnace chamber [10–12] and even with 2D simplifications, there are only a few reports with regard to 3D, full-loop simulation of CFBs

* Corresponding author. Tel.: +86 10 82616050; fax: +86 10 62558065.
E-mail address: wangwei@home.ipe.ac.cn (W. Wang).

1385-8947/$ – see front matter © 2010 Elsevier B.V. All rights reserved.
doi:10.1016/j.cej.2010.06.033

Nomenclature

C_d	drag coefficient
d_s	particle diameter (m)
e_{ss}	coefficient of restitution for particle collisions
g	gravitational acceleration (m/s^2)
g_0	radial distribution function, dimensionless
G_s	solid flux (kg/(m^2 s))
H_d	heterogeneity index of the drag coefficient correction
I_{2D}	second invariant of the deviatoric stress tensor
p	pressure (Pa)
Re	Reynolds number
U_g	superficial gas velocity (m/s)
v	real velocity (m/s)

Greek letters

α	volume fraction
γ_{Θ_s}	collisional dissipation of energy (kg/(m s^3))
β	interphase momentum exchange coefficient derived from EMMS/matrix (kg/(m^3 s))
β_0	interphase momentum exchange coefficient derived from Wen and Yu [20] (kg/(m^3 s))
Θ_s	granular temperature (m^2/s^2)
k_{Θ_s}	diffusion coefficient of energy (kg/(m s))
λ	bulk viscosity (kg/(m s))
μ	shear viscosity (kg/(m s))
ρ	density (kg/m^3)
$\boldsymbol{\tau}$	stress–strain tensor (Pa)
ϕ	angle of internal friction (°)

Subscripts

g	gas phase
s	solid phase

[13–15]. To better understand the CFB boiler behavior, we need detailed information in terms of, for example, the dynamic mixing of gas and solid fuels both horizontally and vertically, the effects of various non-uniform geometries such as coal-feed inlets, solid-return valves and secondary air-injection nozzles, and the pressure balance over the whole loop of CFB circulation. All these considerations necessitate *3D, full-loop CFD simulations*, which may even be viewed as "virtual experimentation" if with reliable models. A recent attempt of us has showed the advantages of such virtual experimentation with detailed validation against experimental data on a pilot-scale cold-model CFB [15]. This paper is to extend our experience on virtual experimentation to investigate the hydrodynamics around the entire loop of an industrial 150 MW$_e$ CFB boiler. Simulation results were showed in terms of profiles of solids distribution, non-uniform distribution of solid fluxes into two parallel cyclones and so on. This work can be expected to help better understand the overall behavior of CFB boilers.

2. Model

2.1. Governing equations

The Eulerian granular model in Fluent®6.3.26 was used to study the flow behavior in the boiler, in which the stress of the solid phase was described with the kinetic theory of granular flow; the drag coefficient correlation was corrected with consideration of particle clusters. More details of the governing equations can be found in Appendix A.

2.2. Drag coefficient correlation

Under the framework of the EMMS model [16], the heterogeneous gas–solid flow in each grid was characterized with the solid-rich dense phase, the gas-rich dilute phase and their meso-scale interface. The effective gas–solid momentum exchange owing to this sub-grid structure is lower than that for uniform suspensions [17–19]. To characterize this structure-induced decrease, Wang and Li [18] defined a heterogeneity index H_d as:

$$H_d \equiv \frac{\beta}{\beta_0},$$

where β is the interphase momentum exchange coefficient calculated from EMMS/matrix model, and β_0 is the interphase momentum exchange coefficient derived from Wen and Yu [20] for uniformly distributed particles, as follows:

$$\beta_0 = \frac{3}{4} C_d \frac{\alpha_s \alpha_g \rho_g |\mathbf{v}_s - \mathbf{v}_g|}{d_s} \alpha_g^{-2.65}.$$

Table 1 summarizes the fitted correlation of H_d for a typical set of operating conditions. This H_d was obtained by using the two-step scheme of EMMS/matrix model [18,21], and the cluster diameter d_{cl}, one of the key parameters therein, was obtained using the method in reference [19]. The two-step scheme here was used to save time, and the drag coefficient from EMMS/matrix can also be coupled into the Eulerian granular model directly during the calculation.

2.3. Geometry and mesh

The 150 MW$_e$ CFB boiler was designed by Harbin Boiler Co. Ltd. and installed in Guangdong, China. It was a natural-circulation, 480 t/h boiler, as shown in Fig. 1, mainly consisting of a furnace, two high-temperature adiabatic cyclone separators and naturally-balanced U-type return valves. The main cross section of the furnace is a rectangle of 15.32 × 7.22 m^2; the chamber height is 36.5 m; the diameter of the two cyclones is 8.08 m; each return leg is connected with a return valve, through which the solid materials are distributed into two pipes, each with a coal-feed inlet, back to the furnace. Besides the primary air inlets from the bottom, there are 26 secondary air inlets located at the inclined bottom walls, two at each side walls, the other 22 distributed at three heights of the front and the back walls. In addition, two slag-cooler inlets are located at the front of the inclined bottom wall.

The simulation domain covers the whole loop of the solid material as shown in Fig. 1. For convenience, the primary air was assumed to enter the furnace in plug flow from the whole bottom of the furnace and the loop-seal aeration was also simplified into plug flow from its bottom. The solid materials exiting from the cyclone outlets were returned via the coal-feed inlets to balance the solid inventory in the boiler.

The boiler was divided into several blocks, in which e.g. the connections between air inlets and the furnace were meshed with polyhedron, and the others were meshed with hexahedron, all with size scale of 0.1 m. The surface mesh is shown in Fig. 2. The origin point is set at the center of the primary inlet at the bottom of the furnace; the x-axis is along the front-to-back wall direction (width direction); the y-axis is along the side-to-side wall direction (depth direction), and the z-axis is against the gravity direction.

2.4. Simulation settings

The boiler was considered operated at the design temperature of 917 °C, and atmospheric pressure, which means that the gas phase was set with a density of 0.2928 kg/m^3 and a viscosity of 4.71 × 10^{-5} kg/(m s). The solid phase was set with a diameter of

Table 1
Heterogeneity index calculated for a CFB boiler with (U_g = 5.25 m/s, G_s = 5 kg/(m^2 s), d_s = 0.2 mm), $H_d = A(Re+B)^C/H_{d,max}$, $H_{d,max}$ = 1.376.

$0.65 < \alpha_g \leq 0.712$	$A = -0.70 + 3.35 \times \alpha_g - 5.36 \times \alpha_g^2 + 2.93 \times \alpha_g^3$ $B = 107.42 - 509.47 \times \alpha_g + 799.18 \times \alpha_g^2 - 414.05 \times \alpha_g^3$ $C = 3.87 - 16.80 \times \alpha_g + 29.54 \times \alpha_g^2 - 17.62 \times \alpha_g^3$
$0.712 < \alpha_g \leq 0.976$	$A = 0.99 - 2.09 \times \alpha_g + 0.08 \times \alpha_g^2 + 1.33 \times \alpha_g^3$ $B = 25.28 - 79.46 \times \alpha_g + 83.31 \times \alpha_g^2 - 29.12 \times \alpha_g^3$ $C = 0.91 + 4.52 \times \alpha_g - 11.89 \times \alpha_g^2 + 6.76 \times \alpha_g^3$
$0.976 < \alpha_g \leq 0.998$	$A = 22899.63 - 69915.92 \times \alpha_g + 71155.28 \times \alpha_g^2 - 24138.87 \times \alpha_g^3$ $B = 53478.28 - 162356.87 \times \alpha_g + 164292.53 \times \alpha_g^2 - 55413.85 \times \alpha_g^3$ $C = -39578.26 + 120883.43 \times \alpha_g - 123073.51 \times \alpha_g^2 + 41768.94 \times \alpha_g^3$
$\alpha_g \leq 0.65$ or $\alpha_g > 0.998$	$H_d = 1$

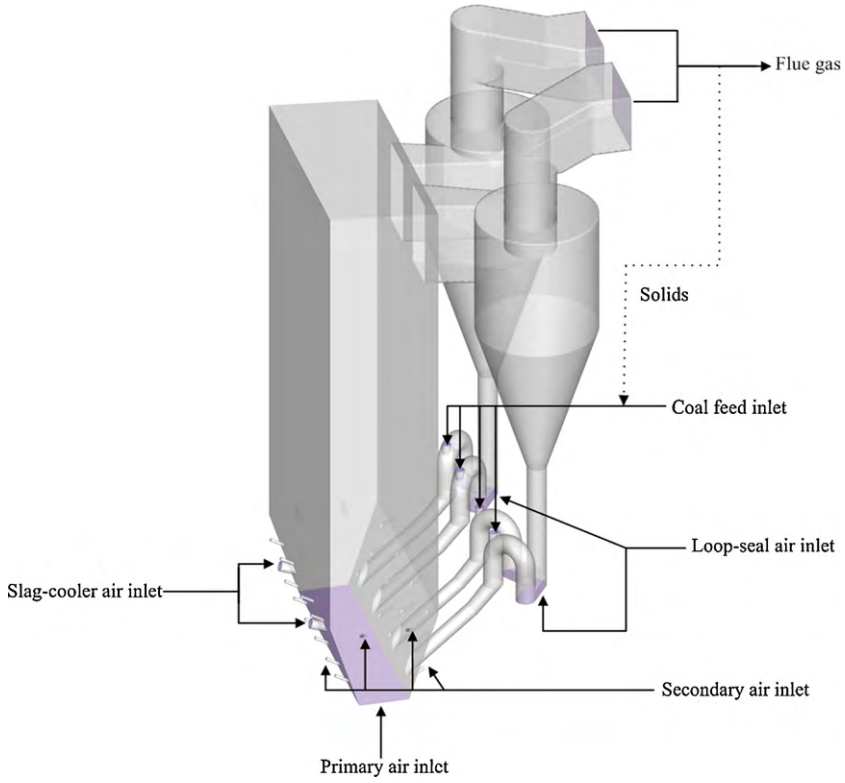

Fig. 1. Geometry of the whole loop of the 150 MW$_e$ CFB boiler.

0.2 mm and a density of 2000 kg/m^3 based on empirical data [11]. Table 2 summarizes solids properties and Table 3 the boundary and initial conditions. The gas velocities at different inlets were set according to the designed gas flow rates, while the solids velocities at the coal-feed inlets were set according to the solid fluxes predicted at the two cyclone outlets by using UDF. At the cyclone outlets, atmospheric pressure was prescribed. At the walls, the no-slip boundary condition was used for the gas phase and a partial slip model [22] was selected with a specularity coefficient of 0.6 for the solid phase. It is difficult to precisely estimate the initial packing height of solids for a given pressure drop, Δp, because the solid materials in the return legs and cyclones are difficult to budget. By trials and errors, in this work the boiler was initially packed with solids volume fraction of 0.4 and packing height of 2.5 m in both the furnace and the two return legs. If not specified, default values in Fluent®6.3.26 were used for the other parameters.

Table 2
Solids properties.

Properties	Setting
Density	2000 kg/m^3
Diameter	2×10^{-4} m
Granular temperature	Phase property[a]
Granular viscosity	Gidaspow[a]
Granular bulk viscosity	Lun et al.[a]
Frictional viscosity	Schaeffer[a]

[a] Optional items of solids properties in Fluent®6.3.26.

2.5. Solution

The Phase Coupled SIMPLE method was chosen for pressure–velocity coupling, the first-order upwind scheme was used for discretization of momentum and volume-fraction equations. The time step size was 0.0005 s. The solid fluxes at the outlets of the two cyclones were monitored to judge when the simulation reaches steady state, thereafter the time averaging was performed. In general, simulations lasted for about 40 s in physical time and the last 20 s were used for time averaging in our analysis.

Table 3
Boundary and initial conditions.

Boundary and initial conditions	Gas phase			Solid phase
	Flow rate (kg/s)	Total area (m^2)	Inlet velocity (m/s)	
Primary air inlet	94.16	50.88	6.32	0
Secondary air inlet	53.21	0.92	198.01	0
Slag-cooler inlet	8.00	0.75	36.32	0
Loop-seal inlet	2.32	8.02	0.99	0
Coal-feed inlet	12.48	1.16	36.70	UDF
Initial solid packing height				2.5 m
Cyclone outlet		Atmospheric pressure		
Wall		No-slip		Partial slip

3. Results and discussion

3.1. Pressure distribution

Fig. 3 shows the simulated pressure balance in the boiler. It is obvious that the pressure gradient is large at the bottom and comparatively small at the top in the furnace, and the largest gradient occurs at the return legs, which agrees qualitatively with empirical knowledge [23]. As there is no measured data of hydrodynamics over this commercial boiler, for a rather rough comparison, the pressure distribution data from the furnace of another boiler [11,24], which is similar in size to this one, are plotted in Fig. 4 against the simulation results. The general trends of their variations were comparable if their reference pressures near the cyclone outlets, i.e., the pressure at the highest measurement position, were made the same.

3.2. Distribution of solids volume fraction

Fig. 5 shows a snapshot of the simulated solids volume fraction distribution with several slices in vertical (Fig. 5(a)) and horizontal (Fig. 5(b)) directions, respectively. Fig. 5(a) confirms the results shown in Fig. 3, that is, dense bottom coexisting with dilute top in both the furnace chamber and the return legs. Fig. 5(b) shows that the solids volume fraction was normally large near the wall and small in the center of the furnace.

Fig. 6 shows profiles of solids volume fraction at different heights with *y*-averaged values along width (*x*-) direction (Fig. 6(a)) and *x*-

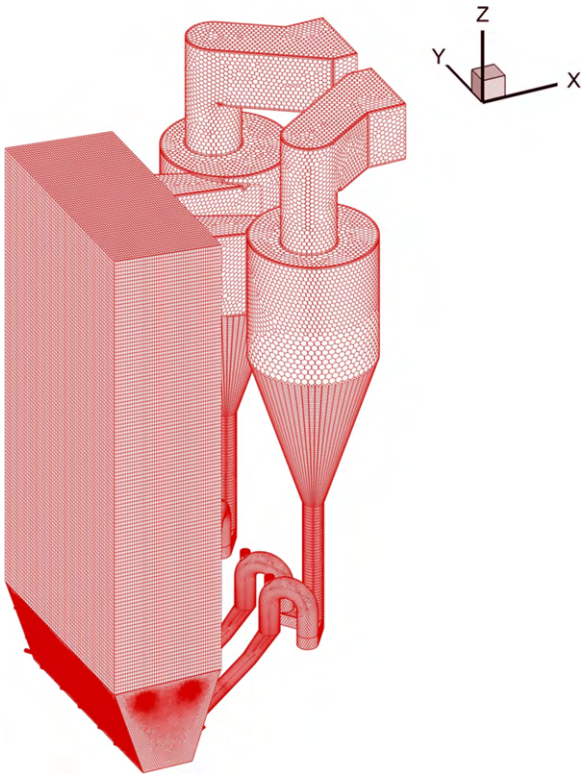

Fig. 2. Surface mesh of the 3D CFB boiler.

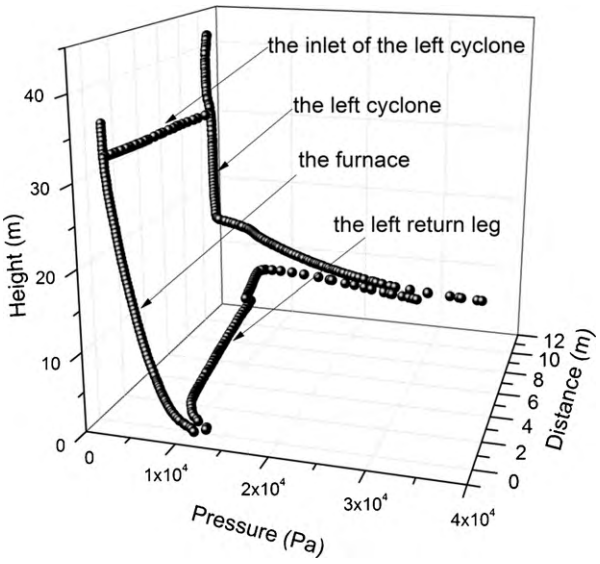

Fig. 3. Simulated pressure balance in the boiler system (simulated pressure data were taken from the center line across the furnace, the left cyclone, its return leg and its left return pipe).

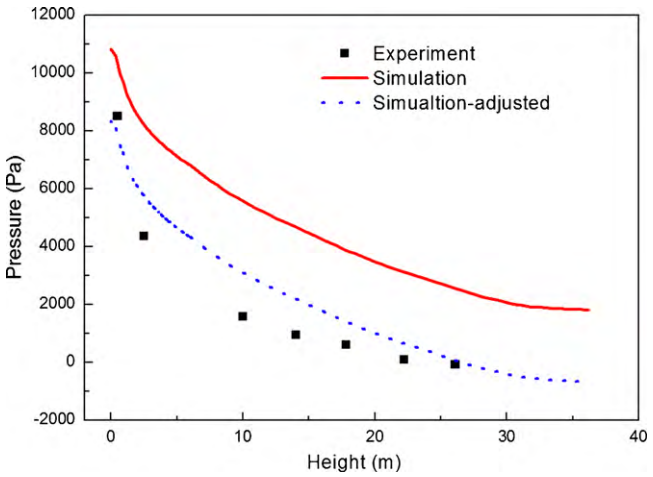

Fig. 4. Comparison of pressure profiles in the furnace between simulation and experiment (Experimental data were obtained from the reference [11] for another boiler, while the simulation-adjusted means that the pressure baseline was adjusted to the same level with the experimental.)

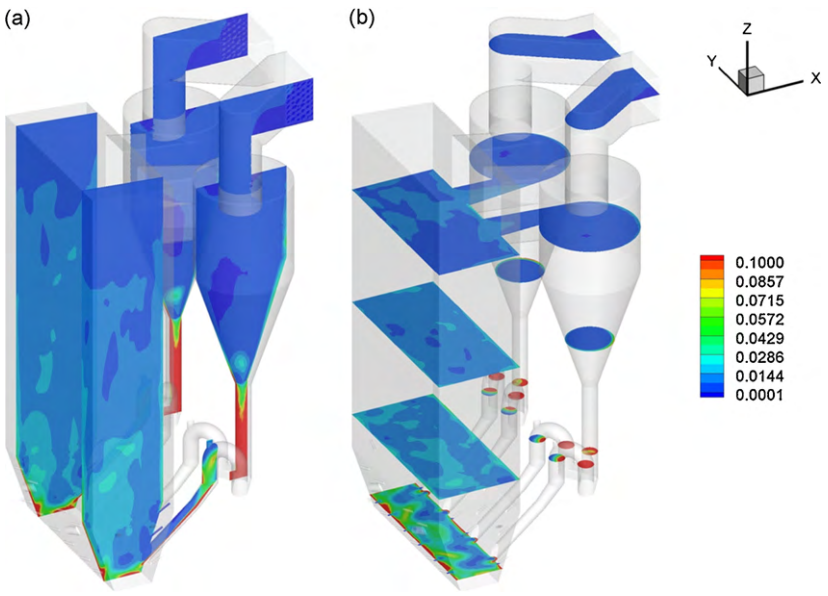

Fig. 5. Simulated solids volume fraction distributions with (a) vertical slices and (b) horizontal slices.

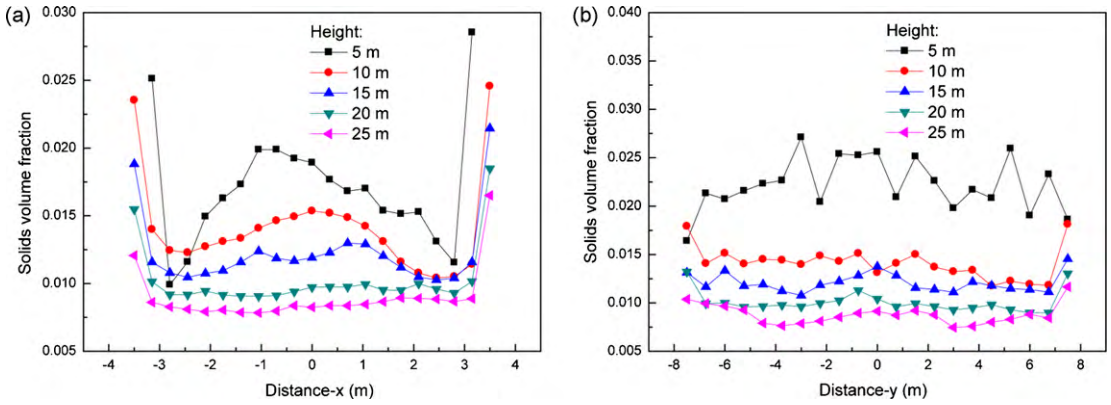

Fig. 6. Profiles of solids volume fraction at different heights with (a) *y*-averaged values along width (*x*-) direction and (b) *x*-averaged values along depth (*y*-) direction.

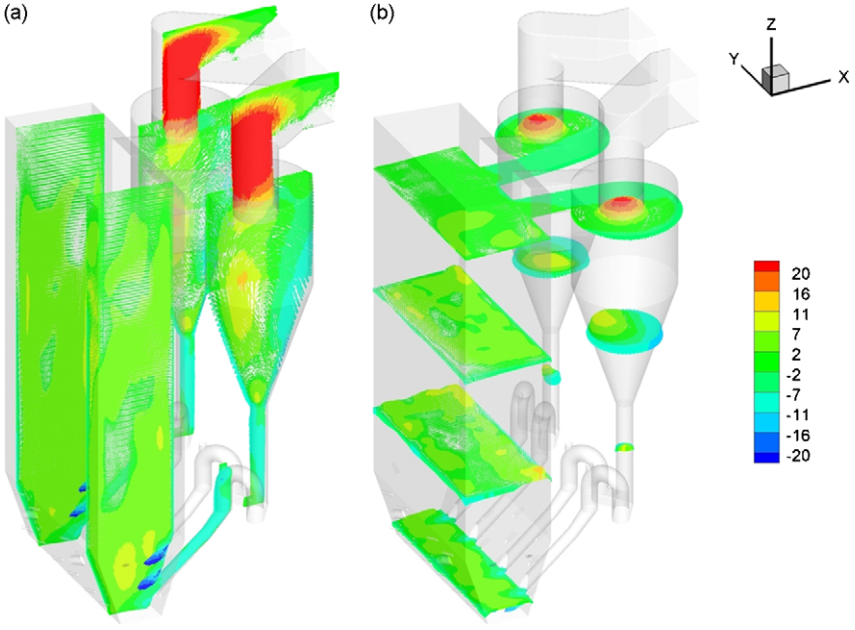

Fig. 7. Simulated solids vertical velocity distribution with (a) vertical slices and (b) horizontal slices.

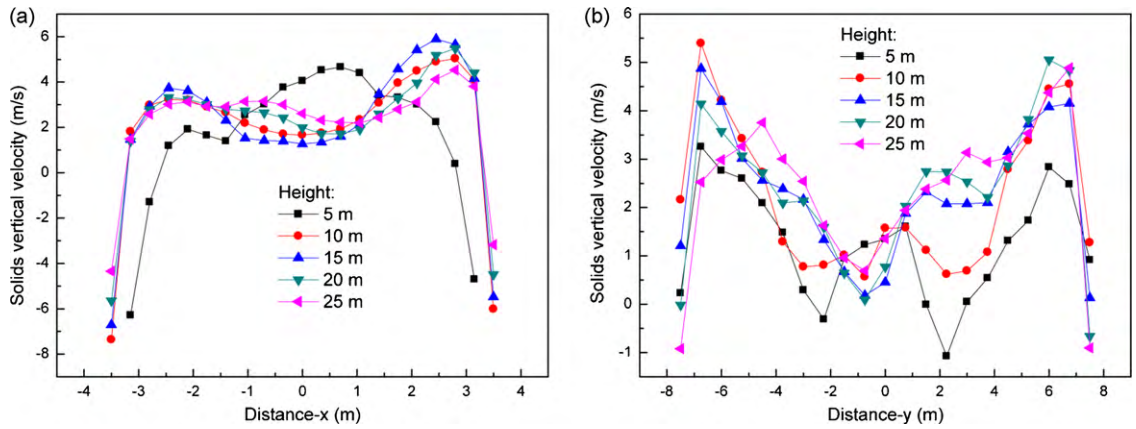

Fig. 8. Profiles of solids vertical velocity at different heights with (a) *y*-averaged values along width (*x*-) direction and (b) *x*-averaged values along depth (*y*-) direction.

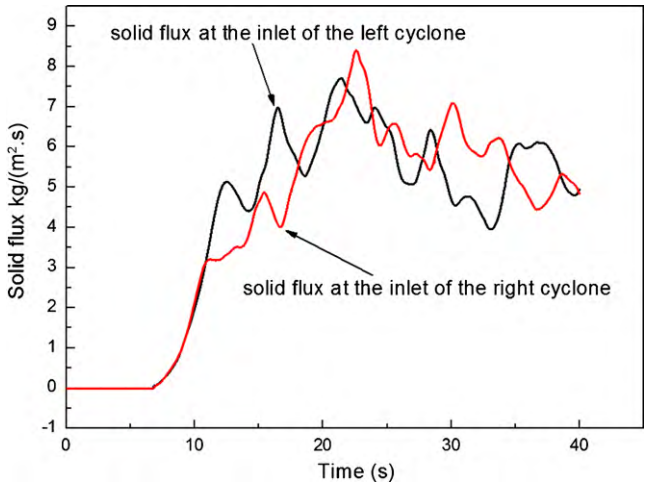

Fig. 9. Comparison of simulated solid fluxes at the cyclone inlets. The flux values were area-averaged fluxes at the inlets of the cyclones, i.e., the back wall of the furnace.

averaged values along depth (*y*-) direction (Fig. 6(b)), respectively. The curves in Fig. 6(a) are typical to the so-called core–annulus structure, showing comparatively dense solids concentration near the wall than in the center. Fig. 6(b) shows different profiles along the depth direction, which are flatter than those along the width direction. This implies that a 2D, *x*–*z* plane simulation may act as a reasonable simplification to the real 3D case. However, we can still see that this 2D reduction will be violated greatly at the dense bottom with significant fluctuation of solids concentration at the height around 5 m, which may be induced by the non-uniform solids recycling inlets.

3.3. Distribution of solids vertical velocity

Fig. 7 shows the simulated distribution of solids vertical velocity with several slices in vertical (Fig. 7(a)) and horizontal (Fig. 7(b)) directions, respectively. Fig. 7(a) shows that vortices can be formed in the furnace and the solids velocity can be significantly affected by the injected air near the secondary air inlet. Fig. 7(b) shows that the solids vertical velocity is mainly positive in the center and negative near the wall. The comparison among these slices seems confirms

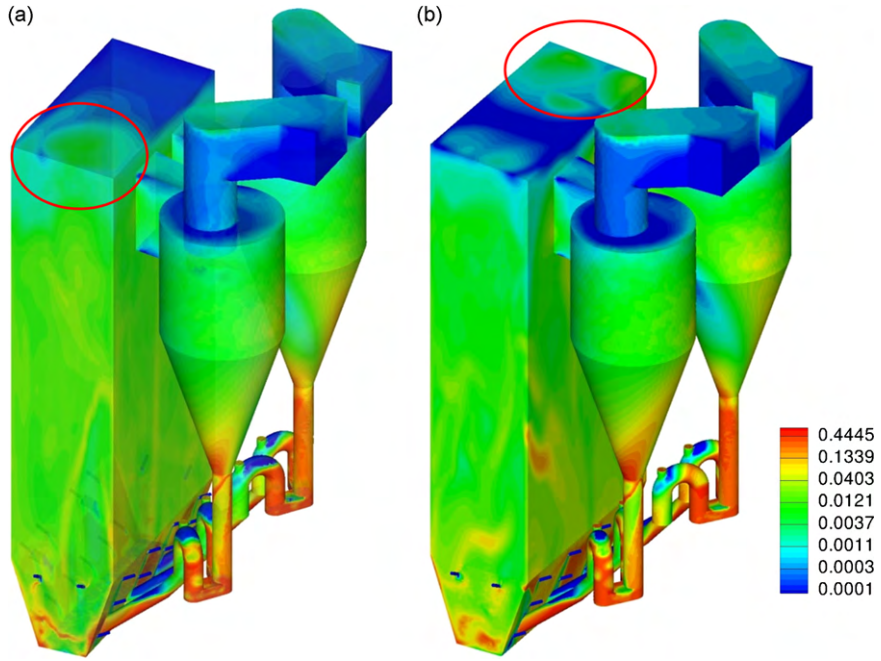

Fig. 10. Instantaneous solids volume fraction distribution in the boiler at simulation time of (a) no. 28.9 s and (b) no. 38.7 s. The red circles indicate high solids volume fraction on the top wall of the furnace. (For interpretation of the references to color in this figure legend, the reader is referred to the web version of the article.)

that the negative velocity near the wall owing to clustering of particles drops with the increase of height.

The results depicted in Fig. 8 are more complex than those in Fig. 6. The core–annulus structure can be confirmed in Fig. 8(a), showing falling clusters near the front- or back walls while rising particles in the center. However, the solids velocity profiles are more fluctuating along the depth-wise direction in the sense that the x-averaged solids velocity may be positive or negative near the side walls; the two maximum rising velocities seems to be affected by two cyclones greatly and their positions deviate much from the center (Fig. 8(b)). As a summary to the results of Figs. 6(b) and 8(b), we can see that the depth-wise flow distribution is hardly uniform and then a 2D simulation cannot be viewed as a reliable simplification to the real 3D case. However, it should be noted that the fluctuating velocity in Fig. 8 might be a result of the averaging time due to limited computing capacity. Real process may take minutes and even hours to reach the steady-state operation. More tests should be performed concerning this phenomenon.

3.4. Solid fluxes at cyclone inlets

As addressed by Grace et al. [25], "when two-phase suspensions are conveyed through identical parallel flow paths, the flow distribution can be significantly non-uniform in practice". This phenomenon has been verified in experiments [26–29]. Measurement of solid flux is difficult for experiments especially on a commercial CFB boiler, but it is easy for simulations. Fig. 9 shows the monitored solid fluxes in this simulation at these two cyclones. In average, the solid fluxes at these two cyclones show minor difference, which are 5.74 kg/(m^2 s) and 6.05 kg/(m^2 s), respectively. Considering the non-uniform solids distribution in the furnace, we can say that the two cyclones operate identically as designed. From the instantaneous point of view, however, the fluxes show a seesaw phenomenon, that is, the maximum flux alternates in these two cyclones; when one cyclone reaches its local maximum flux, the other one is right near its local minimum. Such phenomenon can also be validated, as shown in Fig. 10, from the snapshots of alternate dense accumulation of solids near the cyclone inlets at the top wall. This is the first time that such non-uniform phenomenon is captured with a CFD simulation, which is consistent with Grace's experiment [26]. The current analysis is still at its preliminary level, calling for more systematic work in the future.

4. Conclusions

A 3D, full-loop, time-dependent CFD simulation of a 150 MW$_e$ CFB boiler was performed. It is an extension to our experience on virtual experimentation to investigate the hydrodynamics within an industrial reactor. Simulation results show the capability of the current model, with emphasis on the EMMS-corrected drag coefficient, in predicting the two-phase flow behavior. More simulations can be expected to enable us better understanding CFB boilers.

Acknowledgements

The authors are grateful to Professor Junfu Lu of Tsinghua University for providing the blueprint of the boiler, and to Professor John R. Grace of University of British Columbia for email discussion on the phenomena of parallel cyclones and their efficiency. The financial supports from NSFC under Grant No. 20821092, MOST under Nos. 2007AA050302-03 and 2008BAF33B01, and CAS under No. KGCX2-YW-222 are also greatly acknowledged.

Appendix A. Governing equations

Continuity equations:

$$\frac{\partial}{\partial t}(\alpha_g\rho_g) + \nabla\cdot(\alpha_g\rho_g\mathbf{v}_g) = 0,$$

$$\frac{\partial}{\partial t}(\alpha_s\rho_s) + \nabla\cdot(\alpha_s\rho_s\mathbf{v}_s) = 0.$$

Momentum equations:

$$\frac{\partial}{\partial t}(\alpha_g\rho_g\mathbf{v}_g) + \nabla\cdot(\alpha_g\rho_g\mathbf{v}_g\mathbf{v}_g) = -\alpha_g\nabla p + \nabla\cdot\boldsymbol{\tau}_g + \alpha_g\rho_g\mathbf{g} + \beta(\mathbf{v}_s - \mathbf{v}_g),$$

$$\frac{\partial}{\partial t}(\alpha_s\rho_s\mathbf{v}_s) + \nabla\cdot(\alpha_s\rho_s\mathbf{v}_s\mathbf{v}_s) = -\alpha_s\nabla p - \nabla p_s + \nabla\cdot\boldsymbol{\tau}_s + \alpha_s\rho_s\mathbf{g} + \beta(\mathbf{v}_g - \mathbf{v}_s),$$

Granular energy equation:

$$\frac{3}{2}\left[\frac{\partial}{\partial t}(\rho_s\alpha_s\Theta_s) + \nabla\cdot(\rho_s\alpha_s\mathbf{v}_s\Theta_s)\right] = (-p_s\mathbf{I} + \boldsymbol{\tau}_s) : \nabla\mathbf{v}_s + \nabla\cdot(k_{\Theta_s}\nabla\Theta_s) - \gamma_{\Theta_s} - 3\beta\Theta_s.$$

Constitutive equations:
Stress tensors:

$$\boldsymbol{\tau}_g = \alpha_g\mu_g(\nabla\mathbf{v}_g + \nabla\mathbf{v}_g^T) + \alpha_g\left(\lambda_g - \frac{2}{3}\mu_g\right)\nabla\cdot\mathbf{v}_g\mathbf{I},$$

$$\boldsymbol{\tau}_s = \alpha_s\mu_s(\nabla\mathbf{v}_s + \nabla\mathbf{v}_s^T) + \alpha_s\left(\lambda_s - \frac{2}{3}\mu_s\right)\nabla\cdot\mathbf{v}_s\mathbf{I}.$$

Solid phase pressure:

$$p_s = \alpha_s\rho_s\Theta_s + 2\rho_s(1+e_{ss})\alpha_s{}^2 g_0\Theta_s.$$

Solid phase shear viscosity:

$$\mu_s = \mu_{s,kin} + \mu_{s,col} + \mu_{s,fr},$$

$$\mu_{s,col} = \frac{4}{5}\alpha_s\rho_s d_s g_0(1+e_{ss})\left(\frac{\Theta_s}{\pi}\right)^{1/2},$$

$$\mu_{s,kin} = \frac{10\rho_s d_s\sqrt{\Theta_s\pi}}{96\alpha_s(1+e_{ss})g_0}\left[1 + \frac{4}{5}g_0\alpha_s(1+e_{ss})\right]^2,$$

$$\mu_{s,fr} = \frac{p_s\sin\phi}{2\sqrt{I_{2D}}}.$$

Gas and solid phase bulk viscosity:

$$\lambda_g = 0, \quad \lambda_s = \frac{3}{4}\alpha_s\rho_s d_s g_0(1+e_{ss})\left(\frac{\Theta_s}{\pi}\right)^{1/2}.$$

Radial distribution function:

$$g_0 = \left[1 - \left(\frac{\alpha_s}{\alpha_{s,max}}\right)^{1/3}\right]^{-1}.$$

Diffusion coefficient of energy:

$$k_{\Theta_s} = \frac{150\rho_s d_s\sqrt{(\Theta\pi)}}{384(1+e_{ss})g_0}\left[1+\frac{6}{5}\alpha_s g_0(1+e_{ss})\right]^2 + 2\rho_s\alpha_s{}^2 d_s(1+e_{ss})g_0\sqrt{\frac{\Theta_s}{\pi}}.$$

Collision energy dissipation:

$$\gamma_{\Theta_s} = \frac{12(1-e_{ss}^2)g_0}{d_s\sqrt{\pi}}\rho_s\alpha_s^2\Theta_s^{3/2}.$$

Interphase momentum exchange coefficient:

$$\beta = \frac{3}{4}C_d\frac{\alpha_s\alpha_g\rho_g|\mathbf{v}_s-\mathbf{v}_g|}{d_s}\alpha_g^{-2.65}H_d,$$

where

$$C_d = \frac{24}{\alpha_g Re}[1+0.15(\alpha_g Re)^{0.687}], \quad \text{and} \quad Re = \frac{\rho_g|\mathbf{v}_g-\mathbf{v}_s|d_s}{\mu_g}.$$

References

[1] Y.Y. Lee, T. Hyppanen, A coal combustion model for circulating fluidized bed boilers, in: A.M. Manaker (Ed.), Proceedings of the Tenth International Conference on Fluidized Bed Combustion, vol. 2, ASME, New York, 1989, pp. 753–764.

[2] K. Myöhänen, T. Hyppänen, M. Loschkin, Converting measurement data to process knowledge by using three-dimensional CFB furnace model, in: K. Cen (Ed.), Circulating Fluidized Bed Technology VIII—Proceedings of the Eighth International Conference on Circulating Fluidized Beds, International Academic Publishers, World Publishing Corp., Hangzhou, 2005, pp. 306–312.

[3] K. Myöhänen, T. Hyppänen, Modeling of circulating fluidized bed combustion with a semi-empirical three-dimentional model. Available from: http://www.automaatioseura.fi/confprog/downloadfile_public.php?conference=12&filename=12-12040.pdf (last visited 2010.01.13).

[4] K. Myöhänen, T. Hyppänen, T. Pikkarainen, T. Eriksson, A. Hotta, Near zero CO_2 emissions in coal firing with oxy-fuel circulating fluidized bed boiler, Chem. Eng. Technol. 32 (2009) 355–363.

[5] T. Knoebig, K. Luecke, J. Werther, Mixing and reaction in the circulating fluidized bed—a three-dimensional combustor model, Chem. Eng. Sci. 54 (1999) 2151–2160.

[6] K. Luecke, E.U. Hartge, J. Werther, A 3D model of combustion in large-scale circulating fluidized bed boilers, Int. J. Chem. React. Eng. 2 (2004) A11.

[7] J. Werther, E.U. Hartge, L. Ratschow, R. Wischnewski, Simulation-supported measurements in large circulating fluidized bed combustors, Particuology 7 (2009) 324–331.

[8] D. Pallares, F. Johnsson, Macroscopic modelling of fluid dynamics in large-scale circulating fluidized beds, Prog. Energy Combust. Sci. 32 (2006) 539–569.

[9] D. Pallares, F. Johnsson, Modeling of fuel mixing in fluidized bed combustors, Chem. Eng. Sci. 63 (2008) 5663–5671.

[10] I. Flour, M. Boucker, Numerical simulation of the gas–solid flow in the furnace of a CFB cold rig with ESTET-ASTRID code, in: J.R. Grace, J. Zhu, H. de Lasa (Eds.), Circulating Fluidized Bed Technology VII—Proceedings of the Seventh International Conference on Circulating Fluidized Beds, Canadian Society of Chemical Engineers, Ottawa, 2002, pp. 467–474.

[11] X. Xiao, Multi-dimensional modeling and experimental research on circulating fluidized bed boiler furnace, Ph.D. Dissertation, Tsinghua University, Beijing, 2006.

[12] E.U. Hartge, L. Ratschow, R. Wischnewski, J. Werther, CFD-simulation of a circulating fluidized bed riser, Particuology 7 (2009) 283–296.

[13] K.G. Hansen, J. Madsen, A computational and experimental study of gas–particle flow in a scaled circulating fluidized bed, in: 9th Semester Project, Aalborg Universitet Esbjerg, Esbjerg, 2001.

[14] F. Johnsson, Fluidized bed combustion for clean energy, in: F. Berruti, X. Bi, T. Pugsley (Eds.), Proceedings of the 12th International Conference on Fluidization, ECI Symposium Series, Vancouver, 2007, pp. 47–62, http://services.bepress.com/eci/fluidization_xii/131.

[15] N. Zhang, B. Lu, W. Wang, J. Li, Virtual experimentation through 3D full-loop simulation of a circulating fluidized bed, Particuology 6 (2008) 529–539.

[16] J. Li, M. Kwauk, Particle–Fluid Two-Phase Flow: The Energy-Minimization Multi-scale Method, Metallurgical Industry Press, Beijing, 1994.

[17] N. Yang, W. Wang, W. Ge, J. Li, Choosing structure-dependent drag coefficient in modeling gas–solid two-phase flow, China Particuol. 1 (2003) 38–41.

[18] W. Wang, J. Li, Simulation of gas–solid two-phase flow by a multi-scale CFD approach—extension of the EMMS model to the sub-grid level, Chem. Eng. Sci. 62 (2007) 208–231.

[19] J. Wang, W. Ge, J. Li, Eulerian simulation of heterogeneous gas–solid flows in CFB risers: EMMS-based sub-grid scale model with a revised cluster description, Chem. Eng. Sci. 63 (2008) 1553–1571.

[20] C.Y. Wen, Y.H. Yu, Mechanics of fluidization, Chem. Eng. Prog. Symp. Ser. 62 (1966) 100–111.

[21] B. Lu, W. Wang, J. Li, Searching for a mesh-independent sub-grid model for CFD simulation of gas–solid riser flows, Chem. Eng. Sci. 64 (2009) 3437–3447.

[22] P.C. Johnson, R. Jackson, Frictional–collisional constitutive relations for granular materials, with application to plane shearing, J. Fluid Mech. 176 (1987) 67–93.

[23] P. Herbert, L. Reh, R. Nicolai, The ETH experience: experimental database and results from the past eight years, A.I.Ch.E. Symposium Series No. 321, 95 (1999) 61–66.

[24] X. Xiao, W. Wang, H. Yang, J. Zhang, G. Yue, Two-dimensional combustion modeling of CFB boiler furnace based on an Euler–Euler approach and the kinetic theory of granular flow, in: K. Cen (Ed.), Circulating Fluidized Bed Technology VIII—Proceedings of the Eighth International Conference on Circulating Fluidized Beds, International Academic Publishers, World Publishing Corp., Hangzhou, 2005, pp. 394–401.

[25] J.R. Grace, H. Cui, S.S. Elnashaie, Non-uniform distribution of two-phase flows through parallel identical paths, Can. J. Chem. Eng. 85 (2007) 662–668.

[26] T.-W. Kim, J.-H. Choi, D.W. Shun, B. Jung, S.-S. Kim, J.-E. Son, S.D. Kim, J.R. Grace, Wastage rate of water walls in a commercial circulating fluidized bed combustor, Can. J. Chem. Eng. 84 (2006) 680–687.

[27] T.-W. Kim, J.-H. Choi, D.W. Shun, S.-S. Kim, S.D. Kim, J.R. Grace, Wear of water walls in a commercial circulating fluidized bed combustor with two gas exits, Powder Technol. 178 (2007) 143–150.

[28] M.S. Masnadi, J.R. Grace, S. Elyasi, X. Bi, Distribution of multi-phase gas–solid flow across identical parallel cyclones: modeling and experimental study, Sep. Purif. Technol. (2010), doi:10.1016/j.seppur.2009.12.027.

[29] G. Yue, H. Yang, L. Nie, Y. Wang, H. Zhang, Hydrodynamics of 300 MW_e and 600 MW_e CFB boilers with asymmetric cyclone layout, in: J. Werther, W. Nowak, K.E. Wirth, E.U. Hartge (Eds.), Circulating Fluidized Bed Technology IX—Proceedings of the Ninth International Conference on Circulating Fluidized Beds, TuTech Innovation, Hamburg, Germany, 2008, pp. 153–158.